A Matrix Decomposition MFS Algorithm for Axisymmetric Potential Problems

Yiorgos-Sokratis Smyrlis & Andreas Karageorghis

Department of Mathematics and Statistics
University of Cyprus/ Πανεπιστήμιο Κύπρου, P.O. Box 20537
1678 Nicosia/Λευκωσία, Cyprus/Κύπρος

Abstract

The Method of Fundamental Solutions (MFS) is a boundary-type meshless method for the solution of certain elliptic boundary value problems. By exploiting the structure of the matrices appearing when this method is applied to certain three-dimensional potential problems, we develop an efficient matrix decomposition algorithm for their solution.

1 Introduction

In this study, we apply the Method of Fundamental Solutions (MFS) to axisymmetric potential problems. We investigate the version of the MFS in which the singularities are *fixed* rather than the MFS with *moving* singularities. A description of the various versions of the MFS and related methods, as well as a wide range of applications can be found in the survey papers [4] and [5]. In recent years, the MFS with moving singularities has been used for the solution of a variety of axisymmetric problems [6, 7, 8]. In [11], the MFS with fixed singularities was used for the solution of axisymmetric elastostatics problems. In these applications, the MFS was applied to the axisymmetric version of the governing equations and the fundamental solutions of these equations involve the potentially troublesome evaluation of complete elliptic integrals. Further, when the boundary conditions of the problem under consideration are not axisymmetric, this approach requires the solution of a sequence of problems, in order to evaluate a finite Fourier sum. The approach that we are suggesting in this paper avoids these complications.

We consider the three-dimensional boundary value problem

$$\begin{cases} \Delta u = 0 \quad \text{in} \quad \Omega, \\ \\ u = f \quad \text{on} \quad \partial\Omega\,, \end{cases} \tag{1.1}$$

where Δ denotes the Laplace operator and f is a given function. The region $\Omega \in \mathbb{R}^3$ is axisymmetric, which means that it is formed by rotating a region $\Omega' \in \mathbb{R}^2$ about the z-axis. The boundaries of Ω and Ω' are denoted by $\partial\Omega$ and $\partial\Omega'$, respectively.

2 MFS formulation

In the MFS [4], the solution u is approximated by

$$u_{MN}(\boldsymbol{c}, \boldsymbol{Q}; P) = \sum_{m=1}^{M} \sum_{n=1}^{N} c_{m,n}\, k(P, Q_{m,n}), \qquad P \in \overline{\Omega}, \tag{2.1}$$

where $\boldsymbol{c} = (c_{11}, c_{12}, \ldots, c_{1N}, \ldots, c_{M1}, \ldots, c_{MN})^T$ and $\boldsymbol{Q}$ is a $3MN$-vector containing the coordinates of the singularities (sources) $Q_{m,n}$, $m = 1, \ldots, M,\ n = 1, \ldots, N$, which lie outside $\overline{\Omega}$. The function $k(P, Q)$ is a fundamental solution of Laplace's equation in $\mathbb{R}^3$ given by

$$k(P, Q) = \frac{1}{4\,\pi\,|P - Q|}, \tag{2.2}$$

with $|P - Q|$ denoting the distance between the points P and Q. The singularities $Q_{m,n}$ are fixed on the boundary $\partial\tilde{\Omega}$ of a solid $\tilde{\Omega}$ surrounding Ω. The solid $\tilde{\Omega}$ is generated by the rotation of the planar domain $\tilde{\Omega}'$ which is similar to Ω'. (See *Figures 1,7,10.*) A set of MN collocation points $\{P_{i,j}\}_{i=1,j=1}^{M,N}$ is chosen on $\partial\Omega$ in the following way: We first choose N points on the boundary $\partial\Omega'$ of Ω'. These can be described by their polar coordinates $(r_{P_j},\, z_{P_j})$, $j = 1, \cdots, N$, where r_{P_j} denotes the vertical distance of the point P_j from the z-axis and z_{P_j} denotes the z- coordinate of the point P_j. The points on $\partial\Omega$ are taken to be

$$x_{P_{i,j}} = r_{P_j}\, \cos\varphi_i, \;\; y_{P_{i,j}} = r_{P_j}\, \sin\varphi_i, \;\; z_{P_{i,j}} = z_{P_j},$$

where $\varphi_i = \dfrac{2(i-1)\pi}{M}, \;\; i = 1, \ldots, M\,.$

Similarly, we choose a set of MN singularities $\{Q_{m,n}\}_{i=m,n=1}^{M,N}$ on $\partial\tilde{\Omega}$ by taking $Q_{m,n} = (x_{Q_{m,n}}, y_{Q_{m,n}}, z_{Q_{m,n}})$, and

$$x_{Q_{i,j}} = r_{Q_j}\, \cos\varphi_i, \;\; y_{Q_{i,j}} = r_{Q_j}\, \sin\varphi_i, \;\; z_{Q_{i,j}} = z_{Q_j},$$

where the N points Q_j are chosen on the boundary $\partial\tilde{\Omega}'$ of $\tilde{\Omega}'$.

In the MFS, the coefficients $\boldsymbol{c}$ are determined so that the boundary condition is satisfied at the boundary points $\{P_{i,j}\}_{i=1,j=1}^{M,N}$:

$$u_N(\boldsymbol{c}, \boldsymbol{Q}; P_{i,j}) = f(P_{i,j}), \;\; i = 1, \ldots, M, \; j = 1, \ldots, N. \tag{2.3}$$

This yields an $MN \times MN$ linear system of the form

$$G^0\boldsymbol{c} \;=\; \boldsymbol{f}\,, \tag{2.4}$$

for the coefficients $\boldsymbol{c}$, where the elements of the matrix G^0 are given by

$$G^0_{(i-1)\,N+j,(m-1)\,N+n} = \frac{1}{4\,\pi\,|P_{i,j} - Q_{m,n}|}, \quad i,\, m = 1, \ldots, M, \;\; j,\, n = 1, \ldots, N\,. \tag{2.5}$$

The global matrix G^0 has the *block circulant* structure ([3, 15, 16])

$$G^0 \;=\; \begin{pmatrix} A_1 & A_2 & \cdots & A_M \\ A_M & A_1 & \cdots & A_{M-1} \\ \vdots & \vdots & & \vdots \\ A_2 & A_3 & \cdots & A_1 \end{pmatrix}\,, \tag{2.6}$$

where the matrices $A_\ell,\ \ell = 1, \cdots, M$, are $N \times N$ matrices defined by

$$(A_\ell)_{j,n} = \frac{1}{4\,\pi\,|P_{1,j} - Q_{\ell,n}|}\,, \quad \ell = 1, \ldots, M \quad j,\, n = 1, \ldots, N\,.. \tag{2.7}$$

The system (2.4) can therefore be written as

$$G^0\,\boldsymbol{c} \;=\; \Big(I_M \otimes A_1 + P \otimes A_2 + P^2 \otimes A_3 + \cdots + P^{M-1} \otimes A_M\Big)\,\boldsymbol{c} \;=\; \boldsymbol{f}\,, \tag{2.8}$$

where the matrix P is the $M \times M$ permutation matrix $P = circ\,(0, 1, 0, \cdots, 0)$ and $\otimes$ denotes the matrix *tensor* product.

The tensor (or Kronecker) product of the $m \times n$ matrix V and the $\ell \times k$ matrix W is the $m\,\ell \times n\,k$ matrix

$$V \otimes W \;=\; \begin{pmatrix} v_{11}\,W & v_{12}\,W & \cdots & v_{1n}\,W \\ v_{21}\,W & v_{22}\,W & \cdots & v_{2n}\,W \\ \vdots & \vdots & & \vdots \\ v_{m1}\,W & v_{m2}\,W & \cdots & v_{mn}\,W \end{pmatrix}\,. \tag{2.9}$$

We list the following properties of the tensor product:

(*i*) $V \otimes (W + Z) = V \otimes W + V \otimes Z\,.$

(*ii*) $(V + W) \otimes Z = V \otimes Z + W \otimes Z\,.$

(*iii*) $(V_1 \otimes W_1)\,(V_2 \otimes W_2) = (V_1 V_2) \otimes (W_1 W_2)\,.$

(*iv*) $\text{rank}(V \otimes W) = \text{rank}(V) \cdot \text{rank}(W)\,.$

(*v*) $(V \otimes W)^{-1} = V^{-1} \otimes W^{-1}\,.$

A more comprehensive list of the properties of the tensor product can be found in [9], pages 597-598 or [3], pages 22-23.

2.1 Matrix decomposition algorithm

Matrix decomposition algorithms have been used extensively for the efficient solution of linear systems arizing in the solution of separable elliptic boundary value problems in rectangles with finite difference, finite element or spectral methods. An overview of such algorithms is given in a survey article by Bialecki and Fairweather [1].

A Matrix Decomposition Algorithm involves the reduction of the $MN \times MN$ system (2.8) to M decoupled $N \times N$ systems. This is achieved by exploiting the block circulant structure of G^0 and uses the unitary $M \times M$ Fourier matrix U (i.e. $UU^* = I_M$) which is the conjugate of the matrix (see [3, 15])

$$U^* \;=\; \frac{1}{M^{1/2}} \begin{pmatrix} 1 & 1 & 1 & \cdots & 1 \\ 1 & \omega & \omega^2 & \cdots & \omega^{M-1} \\ 1 & \omega^2 & \omega^4 & \cdots & \omega^{2(M-1)} \\ \vdots & \vdots & \vdots & & \vdots \\ 1 & \omega^{M-1} & \omega^{2(M-1)} & \cdots & \omega^{(M-1)(M-1)} \end{pmatrix},$$

where $\omega = e^{2\pi i/M}$. Premultiplication of a vector $\boldsymbol{x}$ by U (resp. U^*) yields the *Discrete Fourier Transform (DFT)* of $\boldsymbol{x}$ (resp. *Inverse Discrete Fourier Transform (IDFT)* of $\boldsymbol{x}$).

Circulant matrices are diagonalized in the following way. If $C = \operatorname{circ}(c_1, \ldots, c_M)$, then $C = U^*DU$ where $D = \operatorname{diag}(d_1, \ldots, d_M)$, and $d_j = \sum_{k=1}^{M} c_k \omega^{(k-1)(j-1)}$. In particular, the permutation matrix $P = \operatorname{circ}(0, 1, 0, \ldots, 0)$ is diagonalized as $P = U^*DU$ where $D = \operatorname{diag}(d_1, \ldots, d_M)$, $d_j = \omega^{j-1}$.

Further, from the properties of the tensor product

$$(U \otimes I_N)\,(P^{k-1} \otimes A_k)\,(U^\star \otimes I_N) = (UP^{k-1}U^*) \otimes A_k = D^{k-1} \otimes A_k\,, \quad k = 1, \ldots, M.$$

Premultiplication of system (2.8) by $U \otimes I_N$ yields

$$(U \otimes I_N) \left(\sum_{k=1}^{M} P^{k-1} \otimes A_k \right) (U^* \otimes I_N)(U \otimes I_N)\, \boldsymbol{c} \;=\; (U \otimes I_N)\, \boldsymbol{f}\,, \tag{2.10}$$

since $(U^* \otimes I_N)(U \otimes I_N) = I_{MN}$. Therefore,

$$\Big(I_M \otimes A_1 + D \otimes A_2 + D^2 \otimes A_3 + \cdots + D^{M-1} \otimes A_M \Big)\, \tilde{\boldsymbol{c}} \;=\; \tilde{\boldsymbol{f}}\,, \tag{2.11}$$

where $\tilde{\boldsymbol{c}} = (U \otimes I_N)\, \boldsymbol{c}$, $\tilde{\boldsymbol{f}} = (U \otimes I_N)\, \boldsymbol{f}$.

The solution of system (2.11) can therefore be decomposed into the solution of the M *independent* $N \times N$ systems

$$B_m \tilde{\boldsymbol{c}}_m \;=\; \Big(A_1 + d_m\, A_2 + d_m^2\, A_3 + \cdots + d_m^{M-1}\, A_M \Big)\, \tilde{\boldsymbol{c}}_m \;=\; \tilde{\boldsymbol{f}}_m\,, \tag{2.12}$$

where $m = 1, 2, \ldots M$.

The (r, s) entry of the matrix B_m is

$$\begin{aligned}(B_m)_{rs} &= (A_1)_{rs} + d_m\ (A_2)_{rs} + \cdots + d_m^{M-1}\ (A_M)_{rs} \\ &= (A_1)_{rs} + \omega^{m-1}\ (A_2)_{rs} + \cdots + \omega^{(m-1)(M-1)}\ (A_M)_{rs}\ ,\end{aligned}$$

where $r, s = 1, \ldots, N$ and $m = 1, \ldots, M$. Thus we have

$$(\,(B_1)_{rs}, \ldots, (B_M)_{rs})^T \;=\; M^{1/2}\, U^*\ ((A_1)_{rs}, \ldots, (A_M)_{rs})^T\ .$$

This observation enables us to reduce the cost of constructing the matrices $B_1, \ldots, B_M$ from $O(M^2N^2)$ operations to $O(N^2 M \log M)$ operations, using *Fast Fourier Transforms* (FFTs).

We thus have the following matrix decomposition algorithm for solving (2.8):

Algorithm

Step 1. `Compute` $\tilde{\boldsymbol{f}} = (U \otimes I_N)\, \boldsymbol{f}$.

Step 2. `Construct the matrices` $B_m = A_1 + d_m\, A_2 + \cdots + d_m^{M-1}\, A_M$ **,** $m = 1, \ldots, M$.

Step 3. `Solve` $B_m \tilde{\boldsymbol{c}}_m = \tilde{\boldsymbol{f}}_m$, $m = 1, \ldots, M$.

Step 4. `Compute` $\boldsymbol{c} = (U^* \otimes I_N)\, \tilde{\boldsymbol{c}}$.

Remarks

(*i*) In ***Step* 1**, because of the form of the matrix U, the operation is equivalent to performing N DFTs of dimension M. This can done at a cost of $O(NM \log M)$ operations via an appropriate FFT algorithm. Similarly, in ***Step* 4**, because of the form of the matrix U^*, the operation can be carried out via inverse FFTs at a cost of order $O(NM \log M)$ operations.

(*ii*) In ***Step* 2**, for each $r, s = 1, \ldots, N$, we need to perform an M-dimensional inverse FFT, in order to compute the entries $(B_1)_{rs}, \ldots, (B_M)_{rs}$. This can be done at a cost of $O(N^2 M \log M)$ operations.

(*iii*) In ***Step* 3**, we need to solve M complex linear systems of order N. This is done using an LU-factorization with partial pivoting at a cost of $O(M\, N^3)$ operations.

(*iv*) The FFT and inverse FFT operations are performed using the NAG [10] routines `C06FPF`, `C06FQF` and `C06FRF`.

2.2 Rotation of singularities

The singularities can be *rotated* in the φ direction. In particular, we can place the set of MN singularities $\{Q_{m,n}\}_{i=m,n=1}^{M,N}$ on $\partial\tilde{\Omega}$ by taking $Q_{m,n} = (x_{Q_{m,n}}, y_{Q_{m,n}}, z_{Q_{m,n}})$, and

$$x_{Q_{i,j}} = r_{Q_j} \cos\varphi_i, \;\; y_{Q_{i,j}} = r_{Q_j} \sin\varphi_i, \;\; z_{Q_{i,j}} = z_{Q_j},$$

where $\varphi_i = \dfrac{2(\alpha+i-1)\pi}{M}, \quad i = 1,\dots,M$ and $0 \le \alpha < 1$. With this rotation, the block circulant structure of the matrix, which we shall now denote by G^α, is preserved. In particular, we have

$$G^\alpha = \begin{pmatrix} A_1^\alpha & A_2^\alpha & \cdots & A_M^\alpha \\ A_M^\alpha & A_1^\alpha & \cdots & A_{M-1}^\alpha \\ \vdots & \vdots & & \vdots \\ A_2^\alpha & A_3^\alpha & \cdots & A_1^\alpha \end{pmatrix}, \tag{2.13}$$

where the matrices $A_\ell^\alpha, \; \ell = 1,\cdots,M$ are $N \times N$ matrices. Thus the matrix decomposition algorithm described in the previous section is also applicable in this case.

Theorem *When M is even, the matrix $G^{\frac{1}{2}}$ is singular.*

Proof: Let $M = 2m, \; m \in \mathbb{N}$. The matrix $G^{\frac{1}{2}}$ is of the *block circulant form*

$$circ(B_1, B_2, ..., B_m, B_m, B_{m-1}, ..., B_1),$$

where the matrices $B_i = A_i^{\frac{1}{2}} = A_{M-i+1}^{\frac{1}{2}}, \; i = 1,\cdots,m$. We observe that the sum of the m odd block rows of the matrix $G^{1/2}$ is equal to the sum of the m even block rows of $G^{1/2}$ and therefore the matrix $G^{1/2}$ is singular. In particular, each of these sums is a block row consisting of M matrices of order $N \times N$ each of which is equal to the matrix $\sum_{i=1}^m B_i$.
$\square$.

Corollary *When M is even and only one of the singularities Q_j, $j = 1,\dots,N$ on the boundary $\partial\tilde{\Omega}'$ is rotated to $\alpha = \frac{1}{2}$, the resulting matrix is singular.*

Proof: As before let $M = 2m, \; m \in \mathbb{N}$. In this case, the system matrix has an $M \times MN$ submatrix which has the *vector circulant form* $circ(\mathbf{a}_1^T, \mathbf{a}_2^T, ..., \mathbf{a}_m^T, \mathbf{a}_m^T, \mathbf{a}_{m-1}^T, ..., \mathbf{a}_1^T)$, where the vectors $\mathbf{a}_i, \; i = 1,\cdots,m$ are N-vectors. The sum of the m odd rows of this submatrix is equal to the sum of the m even rows of the submatrix, hence the resulting matrix is singular.
$\square$.

3 Examples of axisymmetric solids

3.1 Case I: Spherical domains

We first consider the case where the domain $\Omega \in \mathbb{R}^3$ is the sphere of radius ϱ, defined by

$$\Omega = \{\boldsymbol{x} \in \mathbb{R}^3 \, : \, |\boldsymbol{x}| < \varrho\}. \tag{3.1}$$

In this case, the singularities $Q_{m,n}$ are fixed on the boundary $\partial\tilde{\Omega}$ of a sphere $\tilde{\Omega}$ generated by a semicircle similar to the semicircle generating Ω. This sphere is defined by $\tilde{\Omega} = \{\boldsymbol{x} \in \mathbb{R}^3 : |\boldsymbol{x}| < R\}$ where $R > \varrho$. A set of $M\,N$ collocation points $\{P_{i,j}\}_{i=1,j=1}^{M,N}$ is chosen on $\partial\Omega$, so that if $P_{i,j} = (x_{P_{i,j}}, y_{P_{i,j}}, z_{P_{i,j}})$, then

$$x_{P_{i,j}} = \varrho\, \sin\vartheta_j\, \cos\varphi_i, \quad y_{P_{i,j}} = \varrho\, \sin\vartheta_j\, \sin\varphi_i, \quad z_{P_{i,j}} = \varrho\, \cos\vartheta_j,$$

where $\varphi_i = \dfrac{2(i-1)\pi}{M}$, $\; i = 1, \ldots, M$ and $\vartheta_j = \dfrac{j\,\pi}{N+1}$, $\; j = 1, \ldots, N$. Note that we avoid the points corresponding to $\vartheta_j = 0$ and $\vartheta_j = \pi$ as these remain invariant under rotation in the φ-direction and hence lead to singular matrices.

Similarly, we choose a set of $M\,N$ singularities $\{Q_{m,n}\}_{i=m,n=1}^{M,N}$ on $\partial\tilde{\Omega}$ by taking $Q_{m,n} = (x_{Q_{m,n}}, y_{Q_{m,n}}, z_{Q_{m,n}})$, and

$$x_{Q_{i,j}} = R\, \sin\vartheta_j\, \cos\varphi_i, \quad y_{Q_{i,j}} = R\, \sin\vartheta_j\, \sin\varphi_i,$$
$$z_{Q_{i,j}} = R\, \cos\vartheta_j, \quad i = 1, \ldots, M, \quad j = 1, \ldots, N.$$

A typical MFS discretization of the sphere is shown in Figure 1.

Ideally, the boundary points and singularities could have been distributed uniformly. In the two dimensional case (i.e. the disk), such a distribution is possible for any number of boundary points/singularities since there exists a canonical polygon for each $N \in \mathbb{N}$. In the three dimensional case, however, such a distribution only exists for certain (finitely many) values of N. Efforts to produce a more uniform distribution of the boundary points/singularities, using an algorithm taking into account the surface area corresponding to each boundary point/singularity, revealed little change in the results.

In order to stress the dependence of the MFS system matrix G^0 in (2.4) on the ϑ and φ directions, we shall denote it by $G^{0,0}$. The structure of $G^{0,0}$ is block circulant and the algorithm of Section 1 can be applied for the solution of the MFS system.

The singularities can be *rotated* in both the φ and the ϑ directions. In particular, we can take the set of $M\,N$ singularities $\{Q_{m,n}\}_{i=m,n=1}^{M,N}$ on $\partial\tilde{\Omega}$ by taking $Q_{m,n} = (x_{Q_{m,n}}, y_{Q_{m,n}}, z_{Q_{m,n}})$, and

$$x_{Q_{i,j}} = R\, \sin\vartheta_j\, \cos\varphi_i, \quad y_{Q_{i,j}} = R\, \sin\vartheta_j\, \sin\varphi_i, \quad z_{Q_{i,j}} = R\, \cos\vartheta_j,$$

where $\varphi_i = \dfrac{2(\alpha+i-1)\pi}{M}$, $\; i = 1, \ldots, M$ and $\vartheta_j = \dfrac{(\beta+j)\,\pi}{N+1}$, $\; j = 1, \ldots, N$, $0 \le \alpha, \beta < 1$.
With this rotation, the block circulant structure of the matrix, which we shall now denote by $G^{\alpha,\beta}$ (instead of by G^{α} in (2.13)), is preserved. In particular, we have

$$G^{\alpha,\beta} = \begin{pmatrix} A_1^{\alpha,\beta} & A_2^{\alpha,\beta} & \cdots & A_M^{\alpha,\beta} \\ A_M^{\alpha,\beta} & A_1^{\alpha,\beta} & \cdots & A_{M-1}^{\alpha,\beta} \\ \vdots & \vdots & & \vdots \\ A_2^{\alpha,\beta} & A_3^{\alpha,\beta} & \cdots & A_1^{\alpha,\beta} \end{pmatrix}, \tag{3.2}$$

where the matrices $A_\ell^{\alpha,\beta}$, $\ell = 1, \cdots, M$, are $N \times N$ matrices.

3.2 Case II: Cylindrical domains

We next consider the cylindrical domain $\Omega \in \mathbb{R}^3$ defined by

$$\Omega = \{\boldsymbol{x} = (x, y, z) \in \mathbb{R}^3 \, : \, \sqrt{x^2 + y^2} < \varrho, \;\; -h < z < h\} \, . \tag{3.3}$$

The boundary points $\{P_{i,j}\}_{i=1,j=1}^{M,N}$ are taken to be

$$x_{P_{i,j}} = r_{P_j} \, \cos\varphi_i, \;\; y_{P_{i,j}} = r_{P_j} \, \sin\varphi_i, \;\; z_{P_{i,j}} = z_{P_j},$$

where $\varphi_i = \frac{2(i-1)\pi}{M}$, $i = 1, \ldots, M$ and the polar coordinates (r_{P_j}, z_{P_j}), $j = 1, \cdots, N$, represent N points on the boundary of the rectangle $(0, \varrho) \times (-h, h)$.

Similarly, the MN singularities $\{Q_{m,n}\}_{i=m,n=1}^{M,N}$ are

$$x_{Q_{i,j}} = r_{Q_j} \, \cos\varphi_i, \;\; y_{Q_{i,j}} = r_{Q_j} \, \sin\varphi_i, \;\; z_{Q_{i,j}} = z_{Q_j},$$

where $\varphi_i = \frac{2(i-1)\pi}{M}$, $i = 1, \ldots, M$ and the polar coordinates (r_{Q_j}, z_{Q_j}), $j = 1, \cdots, N$ describe N points on the boundary of the rectangle $(0, R) \times (-H, H)$ with $R > \varrho$ and $H > h$. A typical MFS discretization of the cylinder is shown in Figure 7.

The singularities can be rotated in the φ direction and the block circulant structure of the matrix is preserved.

3.3 Case III: Toroidal domains

We finally consider the case where the domain $\Omega \in \mathbb{R}^3$ is the torus [2] of radii ϱ_1, ϱ_2, $\varrho_2 > \varrho_1$, defined by

$$\Omega = \{\boldsymbol{x} \in \mathbb{R}^3 \, : \, \left(\sqrt{x^2 + y^2} - \varrho_2\right)^2 + z^2 < \varrho_1^2\} \, . \tag{3.4}$$

Its boundary $\partial\Omega$ can be described by the parametric equations

$$x = \varrho_2 \, \cos\varphi + \varrho_1 \, \cos\varphi \, \cos\vartheta, \;\; y = \varrho_2 \, \sin\varphi + \varrho_1 \, \sin\varphi \, \cos\vartheta, \;\; z = \varrho_1 \sin\vartheta,$$

$$0 \leq \varphi \leq 2\,\pi, \;\; 0 \leq \vartheta \leq 2\,\pi. \tag{3.5}$$

The singularities $Q_{m,n}$ are fixed on the boundary $\partial\tilde{\Omega}$ of a torus $\tilde{\Omega}$ similar to Ω and defined by the parametric equations

$$x = R_2 \, \cos\varphi + R_1 \, \cos\varphi \, \cos\vartheta, \;\; y = R_2 \, \sin\varphi + R_1 \, \sin\varphi \, \cos\vartheta, \;\; z = R_1 \, \sin\vartheta,$$

$$\varrho_1 < R_1 < \varrho_2, \;\; R_2 = \varrho_2, \;\; 0 \leq \varphi \leq 2\,\pi, \;\; 0 \leq \vartheta \leq 2\,\pi. \tag{3.6}$$

A set of $M\,N$ collocation points $\{P_{i,j}\}_{i=1,j=1}^{M,N}$ is chosen on $\partial\Omega$, and an equal number of singularities $\{Q_{m,n}\}_{i=m,n=1}^{M,N}$ on $\partial\tilde{\Omega}$. Their coordinates are given by

$$
\begin{aligned}
x_{Q_{m,n}} &= \varrho_2 \cos\varphi_n + \varrho_1 \cos\varphi_n \cos\vartheta_m, \\
y_{Q_{m,n}} &= \varrho_2 \sin\varphi_n + \varrho_1 \sin\varphi_n \cos\vartheta_m, \\
z_{Q_{m,n}} &= \varrho_1 \sin\vartheta_m,
\end{aligned}
$$

and

$$
\begin{aligned}
x_{Q_{m,n}} &= R_2 \cos\varphi_n + R_1 \cos\varphi_n \cos\vartheta_m, \\
y_{Q_{m,n}} &= R_2 \sin\varphi_n + R_1 \sin\varphi_n \cos\vartheta_m, \\
z_{Q_{m,n}} &= R_1 \sin\vartheta_m,
\end{aligned}
$$

where $\vartheta_m = \dfrac{2(m-1)\pi}{N}$, $m = 1, \ldots, M$ and $\varphi_n = \dfrac{2(n-1)\pi}{N}$, $n = 1, \ldots, N$. A typical MFS discretization of the torus is shown in Figure 10.

The singularities can be rotated in both the φ and the ϑ angular directions in following way:

$$
\begin{aligned}
x_{Q_{m,n}} &= R_2 \cos\varphi_n + R_1 \cos\varphi_n \cos\vartheta_m, \\
y_{Q_{m,n}} &= R_2 \sin\varphi_n + R_1 \sin\varphi_n \cos\vartheta_m, \\
z_{Q_{m,n}} &= R_1 \sin\vartheta_m,
\end{aligned}
$$

where $\vartheta_m = \dfrac{2(\beta+m-1)\pi}{N}$, $m = 1, \ldots, M$ and $\varphi_n = \dfrac{2(\alpha+n-1)\pi}{N}$, $n = 1, \ldots, N$ with $0 \le \alpha, \beta < 1$. The resulting matrix is still block circulant.

4 Numerical results

We considered problems of the form (1.1) with the function f corresponding to the exact solutions

Example 1. $u = \cosh(0.3x)\,\cosh(0.4y)\,\cos(0.5z)$.

Example 2. $u = x^2 - 2y^2 + z^2$.

In all the numerical examples reported in this study, we calculated the maximum relative error, i.e. the relative error in the L^∞-norm

$$E = \frac{||u - u_N||_\infty}{||u||_\infty}.$$

Since both the approximate and exact solutions are harmonic functions, so is their difference, and therefore because of the maximum principle, this difference will reach its maximum on the boundary of the domain under consideration. In order to calculate E, it is thus only necessary to evaluate the maximum error on the boundary of the domain. For example, in the case of the sphere, the error was calculated on a grid of boundary points defined by

$$x_{i,j} = \varrho \sin\vartheta_j \cos\varphi_i, \;\; y_{i,j} = \varrho \sin\vartheta_j \sin\varphi_i, \;\; z_{i,j} = \varrho \cos\vartheta_j,$$

where $\varphi_i = \dfrac{2(i-1)\pi}{L}$, $i = 1, \ldots, L$ and $\vartheta_j = \dfrac{j\,\pi}{L+1}$, $j = 1, \ldots, L$ and L is taken to be appropriately large.

4.1 Case I

We considered the sphere with $\varrho = 1$. In Figure 2 we present the logarithm of the maximum relative error E versus the logarithm of the distance R in the case $\alpha = 0$, $\beta = 0$ and for $N(= M) = 16, 24, 32, 48, 64$ and 96 in Example 1. This figure reveals that the MFS approximation is poor when $\epsilon = R - \varrho$ is either very small or very large. Similar observations were reported in the case of the disk [15]. The behaviour of E is very similar in the case when α, $\beta \neq 0$. In Figure 3 we present the corresponding results for Example 2. The behaviour of these results is very similar to the behaviour of the results for Example 1.

In Figure 4 we present the logarithm of the maximum relative error E versus the angular parameter α when $\beta = 0$. Because of the symmetry of the problem about $\alpha = 1/2$, we only considered the values $0 \leq \alpha \leq 1/2$. We present the three cases $\epsilon = R - \varrho = 1, 0.1, 0.01$ for $N(= M) = 8, 12, 16, 24, 32, 48$ and 64 in Example 1. We observe that for $\epsilon = 0.01$ (and smaller) as N increases, the error E is optimized for $\alpha = \frac{1}{6}$. For $\epsilon = 0.1$ the error E is optimized for $\alpha = \frac{1}{4}$ whereas for $\epsilon = 1$ (and larger values of ϵ) E becomes independent of α as N increases. Similar observations were also reported in the case of the disk [15]. The corresponding results for Example 2 are presented in Figure 5 and, as was the case in figures of E versus R, their behaviour is very similar to the results for Example 1.

We also studied the effect of rotating the singularities in the ϑ angular direction. For small values of ϵ, little improvement in E was observed for $0 < \beta < 1$, with the results worsening as $\beta \to 1$. This occurs because of the clustering of the singularities towards the point (-R, 0, 0), which leads to ill-conditioning and hence to poor results. It should also be mentioned that the rotation of the singularities in the ϑ direction creates an imbalance in the distribution of singularities, with more singularities being concentrated near one of the poles of the sphere. Such a rotation could only be useful in cases where it is necessary to place a denser concentration of singularities close to a pole.

A reason for the inaccurate results reported for large R is the poor conditioning of the matrices B_m, $m = 1, 2, \ldots M$ in equation (2.12). An indication of this can be seen from Figure 6 where we present the logarithm of an estimate of the condition number in the L^∞-norm of the matrix B_1 in the case $\alpha = \beta = 0$ versus the logarithm of ϵ, for $N = 8, 16, 32, 64$ and 96. The estimate of the condition number was calculated using the NAG [10] pair `F07ARF-F07AUF`. The behaviour of the condition number of the matrices B_m, $m = 2, 3, \ldots M$ is very similar.

4.2 Case II

We considered the cylinder with $h = 1, \quad \varrho = 1$. We only present results for Example 1 as the results for Example 2 are very similar. In Figure 8 we present the logarithm of the maximum relative error E versus the logarithm of the distance R in the case $\alpha = 0$ and for $N(= M) = 16, 24, 32, 48, 64$ and 96. This figure reveals that, as in the case of the sphere, the MFS approximation is poor when $\epsilon = R - \varrho = H - h$ is either very small or very large. The behaviour of E is very similar when $\alpha \neq 0$.

In Figure 9 we present the logarithm of the maximum relative error E versus the angular parameter α. As before, because of the symmetry of the problem about $\alpha = 1/2$, we only considered the values $0 \leq \alpha \leq 1/2$. We present the three cases $\epsilon = R-\varrho = H-h = 1, 0.1, 0.01$ for various values of $N(= M)$. As in the case of the sphere, for $\epsilon = 0.01$ (and smaller) as N increases, the error E is optimized for $\alpha = \frac{1}{6}$. For $\epsilon = 0.1$ the error E is optimized for $\alpha = \frac{1}{4}$ whereas for $\epsilon = 1$ (and larger values of ϵ), as N increases, E becomes essentially independent of α. In particular, the larger the distance ϵ, the less dependent E is on α.

4.3 Case III

We considered the torus with $\varrho_1 = \frac{1}{2}, \;\; \varrho_2 = 1$. Again, we only present results for Example 1. In Figure 11 we present the logarithm of the maximum relative error E versus the angular parameter α when $\beta = 0$. As before, because of the symmetry of the problem about $\alpha = 1/2$, we only considered the values $0 \leq \alpha \leq 1/2$. We present the three cases $\epsilon = R_1 - \varrho_1 = 0.4, 0.1, 0.02$ for various values of $N(= M)$. Note that in this case, we are restricted in the choice of ϵ. In particular, ϵ has to lie in $(0, \frac{1}{2})$. As in the cases of the sphere and the cylinder, we observe that for $\epsilon = 0.02$ (and smaller), as N increases, the error E is optimized for $\alpha = \frac{1}{6}$. For $\epsilon = 0.1$ the error E is optimized for $\alpha = \frac{1}{4}$ whereas for $\epsilon = 0.4$, E tends to become independent of α as N increases.

In this case we also studied the effect of rotating the singularities in the ϑ angular direction. In Figure 12 we present the logarithm of the maximum relative error E versus the other angular parameter β, when $\alpha = 0$. Because of the symmetry of the problem about $\beta = 1/2$, we only considered the values $0 \leq \beta \leq 1/2$. We consider the two values of $\epsilon = R_1 - \varrho_1 = 0.1$ and 0.02 for various values of $N(= M)$. In this case, we observe that for $\epsilon = 0.02$ (and smaller), as N increases, the optimization point for E tends to $\beta = 1/2$. For $\epsilon = 0.1$, as N increases, E becomes essentially independent of β. Further numerical experiments revealed that for larger values of ϵ E becomes gradually less dependent on β .

5 Conclusions

In this work, we propose an efficient meshless algorithm for the solution of harmonic problems in axisymmetric domains. The algorithm exploits the block circulant structure of the matrices resulting from the MFS discretization of the problem. The ideas developed in this work can also be used when other boundary methods such as the Boundary Element Method are applied to axisymmetric problems; see, for example, [12]. The reason for this is that the structures of the matrices involved in these methods are similar to the structure of the MFS discretization matrices. Further, for the same reason, the proposed algorithm is not restricted to applications of boundary methods to potential problems but can also be used in applications of boundary methods to axisymmetric elasticity and acoustics problems; see, for example, [13] and [14], respectively.

Acknowledgements

The authors wish to thank Professor Graeme Fairweather of the Colorado School of Mines and Professor Efstratios Gallopoulos of the University of Patras for their helpful suggestions.

References

[1] B. Bialecki and G. Fairweather, *Matrix decomposition algorithms for separable elliptic boundary value problems in two space dimensions*, J. Comp. Appl. Math., 46, 369-386, 1993.

[2] H. S. M. Coxeter, *An Introduction to Geometry*, John Wiley and Sons, New York, 1969.

[3] P. J. Davis, *Circulant Matrices*, John Wiley and Sons, New York, 1979.

[4] G. Fairweather and A. Karageorghis, *The method of fundamental solutions for elliptic boundary value problems*, Adv. Comput. Math., 9, 69-95, 1998.

[5] M. A. Golberg and C. S. Chen, *The method of fundamental solutions for potential, Helmholtz and diffusion problems*, in: *Boundary Integral Methods and Mathematical Aspects*, ed. M. A. Golberg, WIT Press/Computational Mechanics Publications, Boston, 1999, pp. 103-176.

[6] A. Karageorghis and G. Fairweather, *The method of fundamental solutions for axisymmetric acoustic scattering and radiation problems*, J. Acoust. Soc. Amer., 104, 3212-3218, 1998.

[7] A. Karageorghis and G. Fairweather, *The method of fundamental solutions for axisymmetric potential problems*, Int. Journal Numer. Meth. in Engng., 44, 1653-1669, 1999.

[8] A. Karageorghis and G. Fairweather, *The method of fundamental solutions for axisymmetric elasticity problems*, Comput. Mech., 25, 524-532, 2000.

[9] C. D. Meyer, *Matrix Analysis and Applied Linear Algebra*, SIAM, Philadelphia, 2000.

[10] *Numerical Algorithms Group Library Mark 20*, NAG Ltd, Wilkinson House, Jordan Hill Road, Oxford, UK, 2001.

[11] D. Redekop and J. C. Thompson, *Use of fundamental solutions in the collocation method in axisymmetric elastostatics*, Comput. & Structures, 17, 485-490, 1983.

[12] F. J. Rizzo and D. J. Shippy, *A boundary integral approach to potential and elasticity problems for axisymmetric bodies with arbitrary boundary conditions*, Mech. Res. Commun., 6, 99-103, 1979.

[13] F. J. Rizzo and D. J. Shippy, *A boundary element method for axisymmetric elastic bodies*, in: *Developments in Boundary Element Methods - 4*, eds. P. K. Banerjee and J. O. Watson, Elsevier, Amsterdam, 1985, pp. 677-690.

[14] A. F. Seybert, B. Soenarko, F. J. Rizzo and D. J. Shippy, *A special integral equation formulation for acoustic radiation and scattering for axisymmetric bodies and boundary conditions*, J. Acoust. Soc. Am., 80, 1241-1247, 1986.

[15] Y.S. Smyrlis and A. Karageorghis, *Some aspects of the method of fundamental solutions for certain harmonic problems*, J. Sci. Comp., 16, 341-371, 2001.

[16] Y.S. Smyrlis and A. Karageorghis, *Some aspects of the method of fundamental solutions for certain biharmonic problems*, Computer Modeling in Engineering & Sciences, to appear.

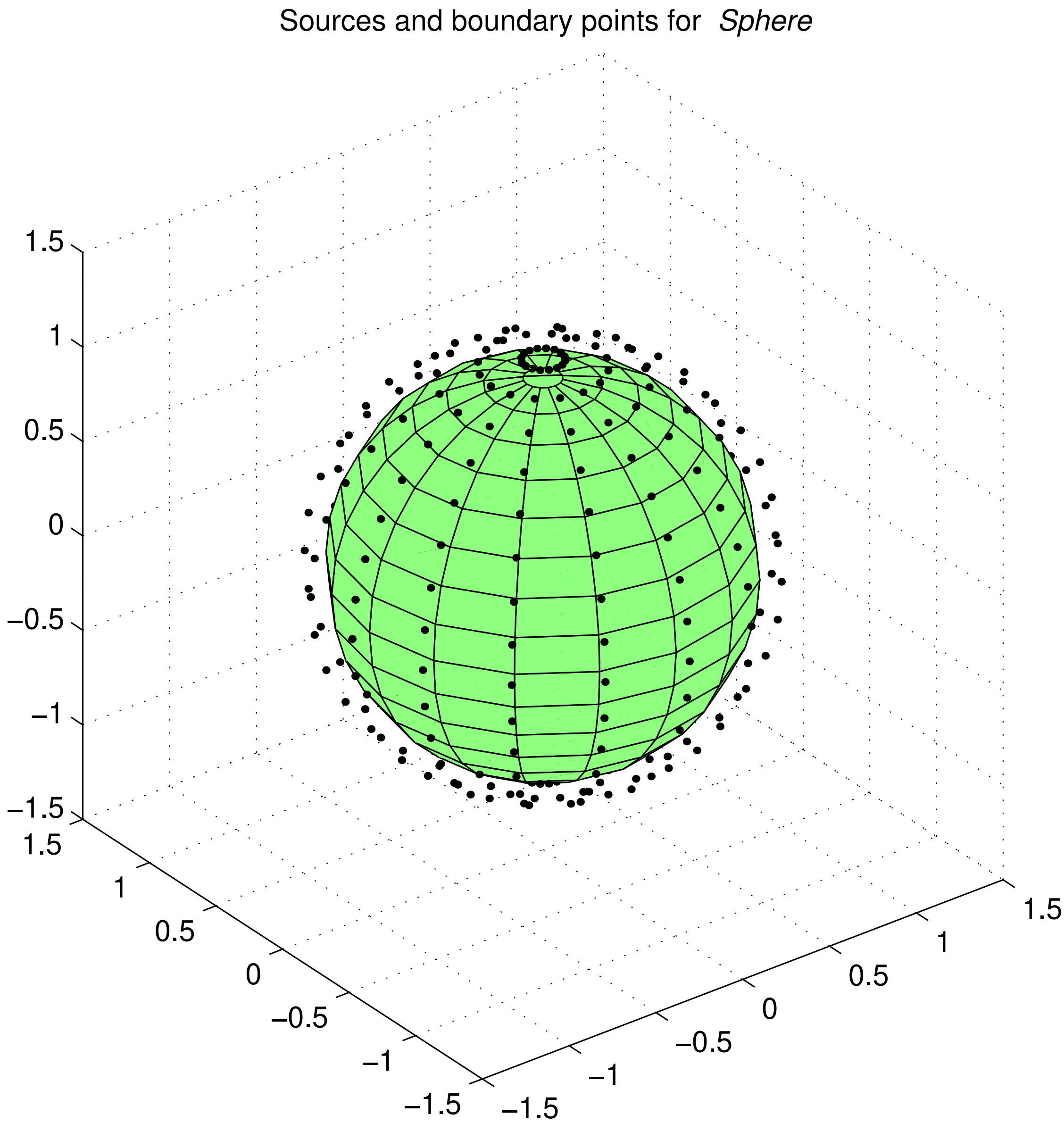

Figure 1: MFS discretization of sphere.

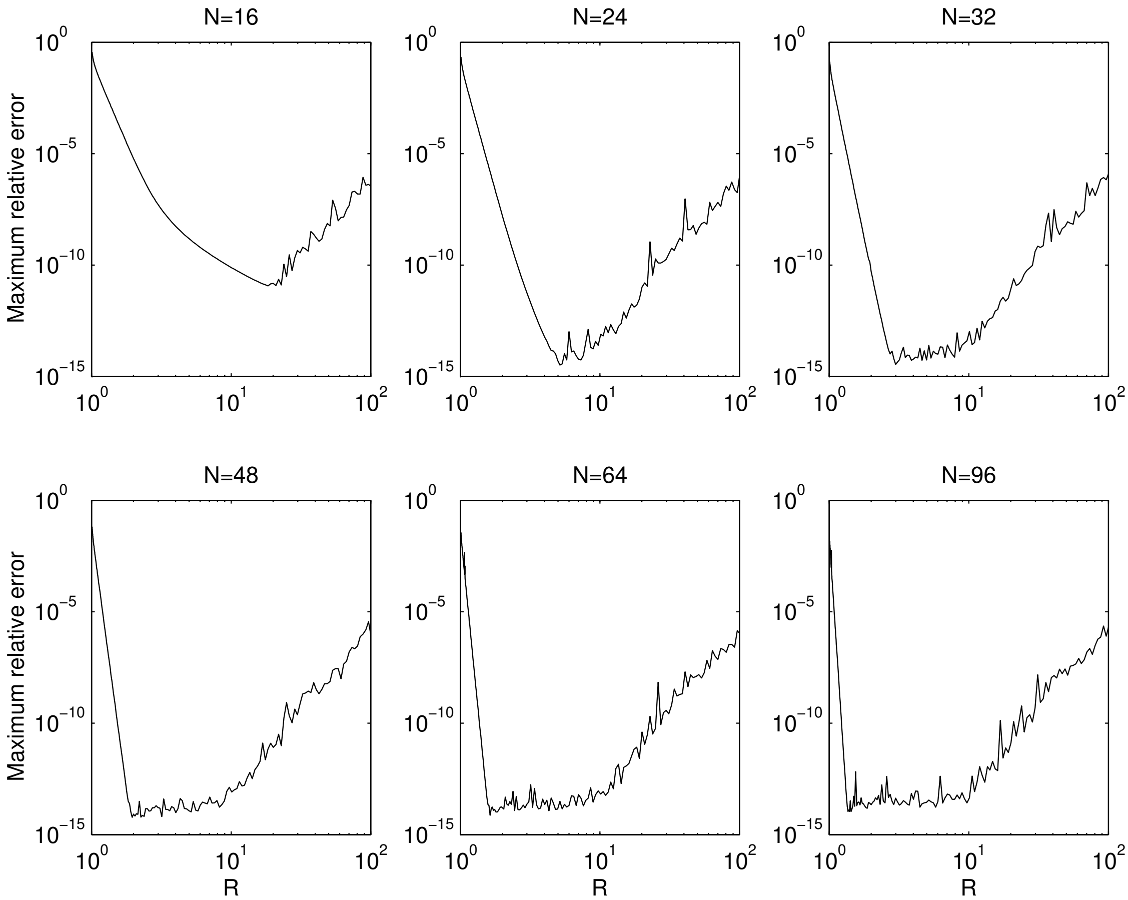

Figure 2: Results for varying distance R and various values of N in the case of the sphere for Example 1.

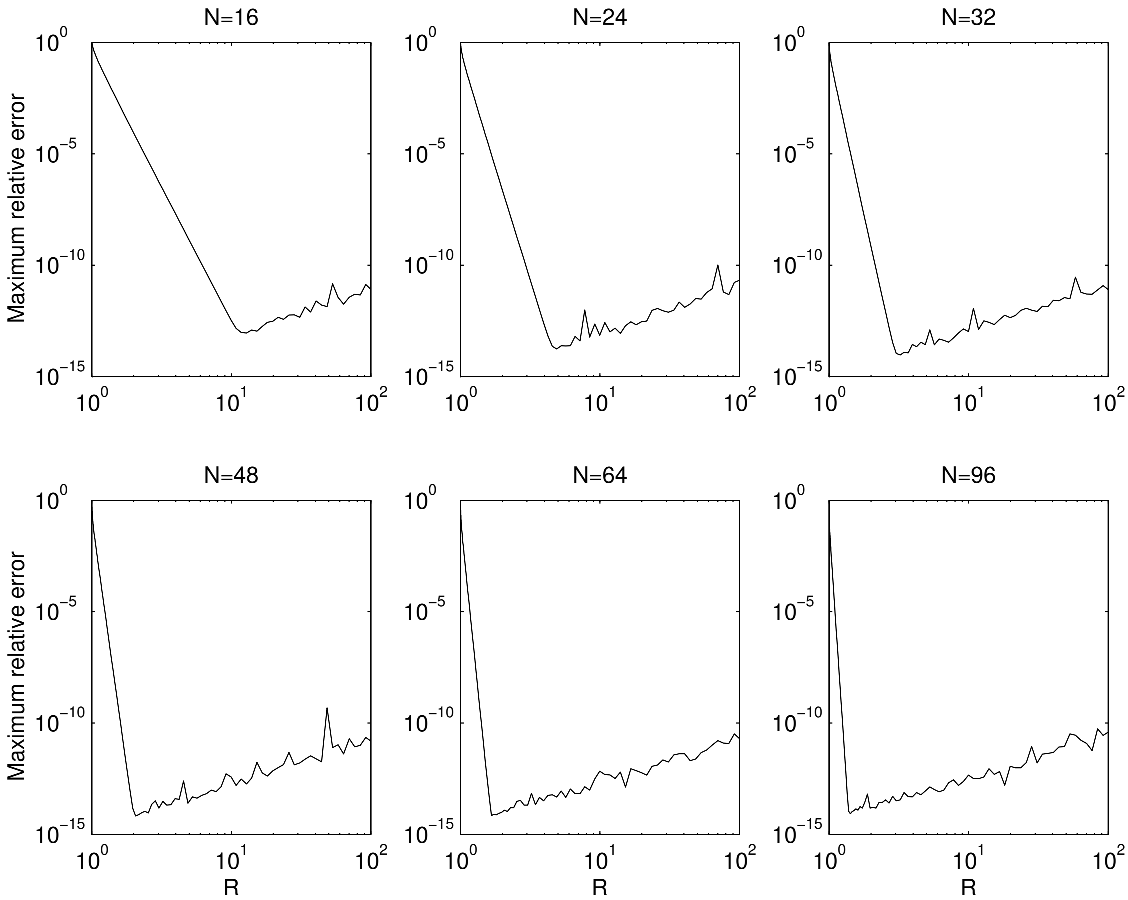

Figure 3: Results for varying distance R and various values of N in the case of the sphere for Example 2.

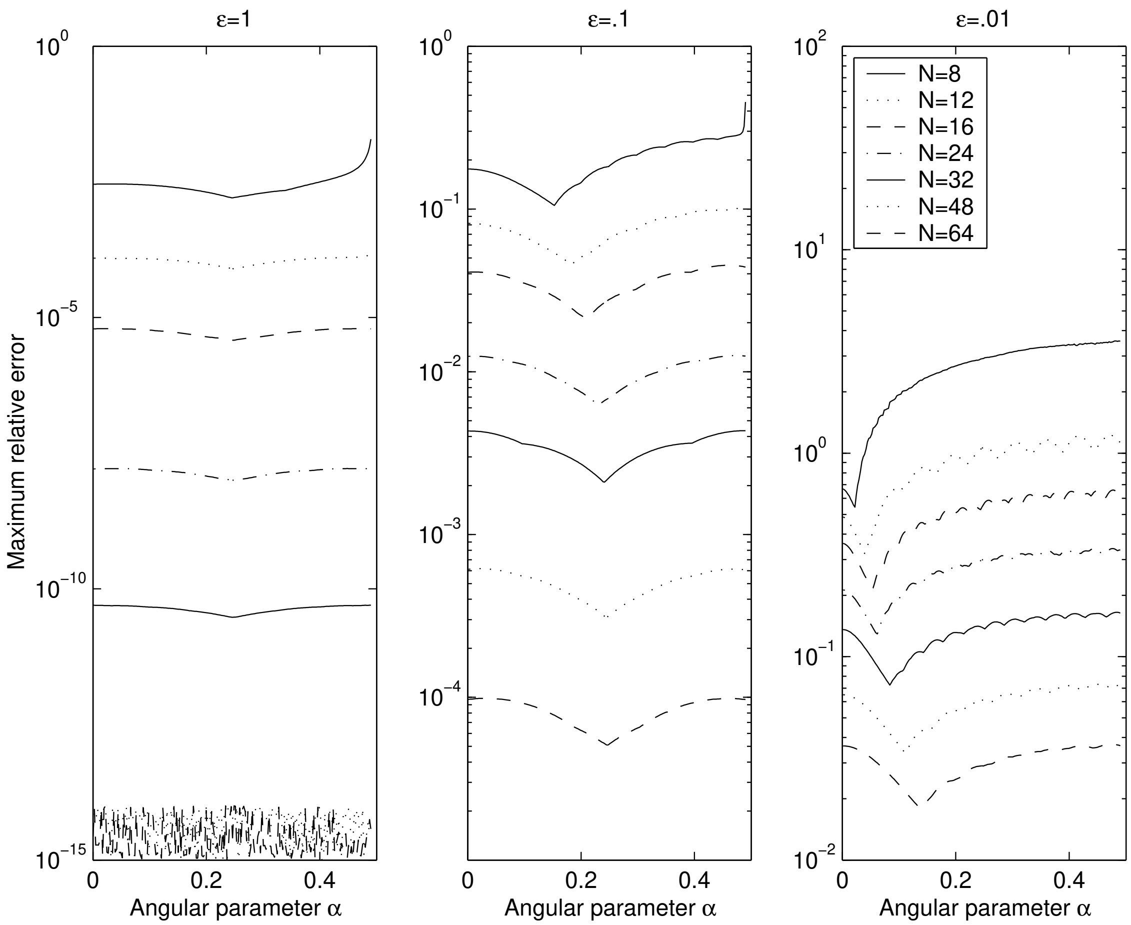

Figure 4: Results for varying parameter α and various values of ϵ in the case of the sphere for Example 1.

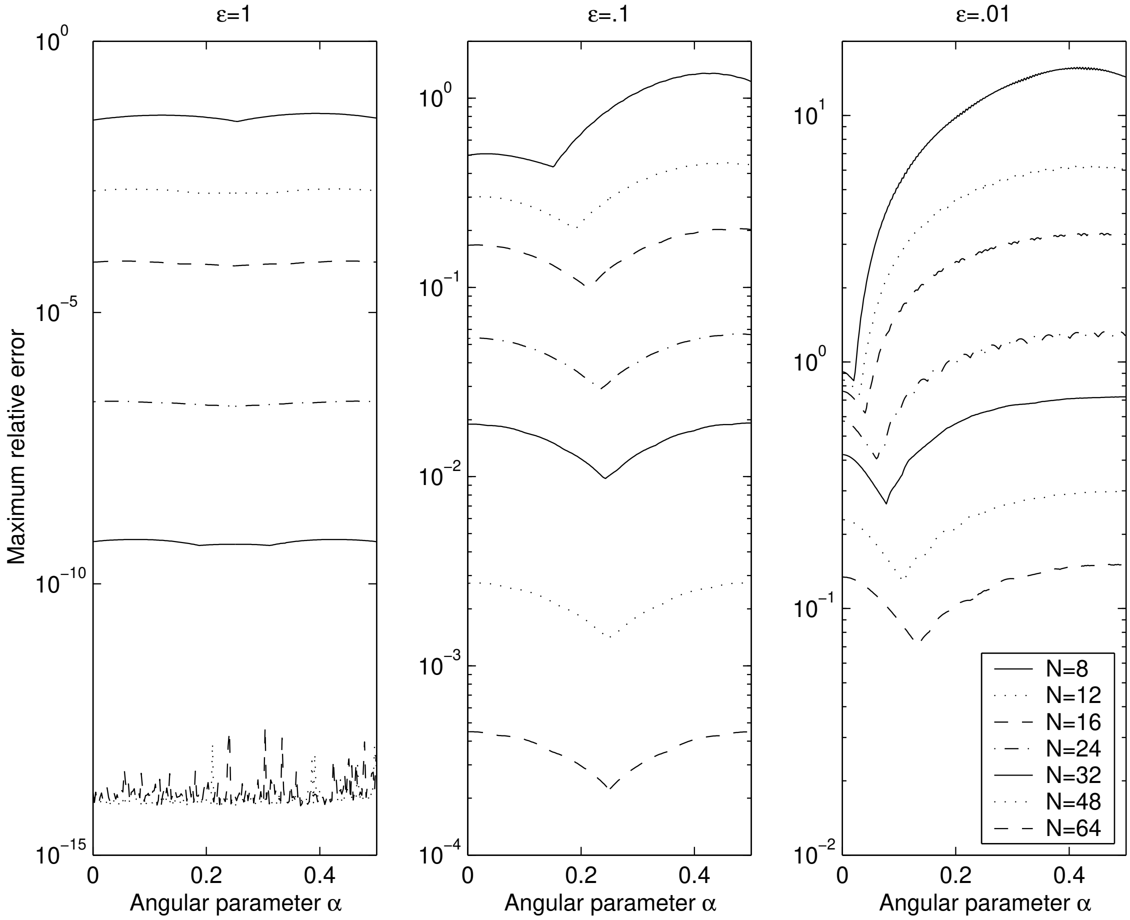

Figure 5: Results for varying parameter α and various values of ϵ in the case of the sphere for Example 2.

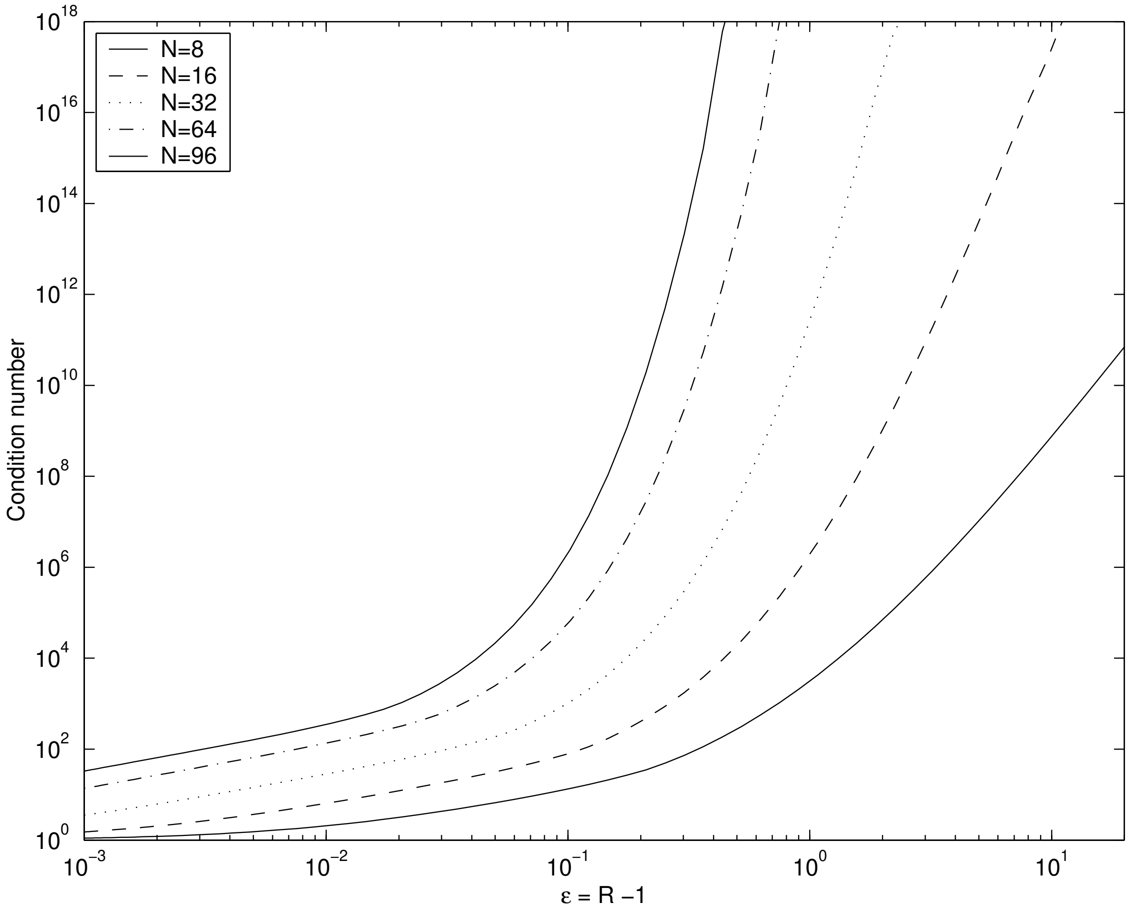

Figure 6: Condition number of matrix B_1 in the case of the sphere.

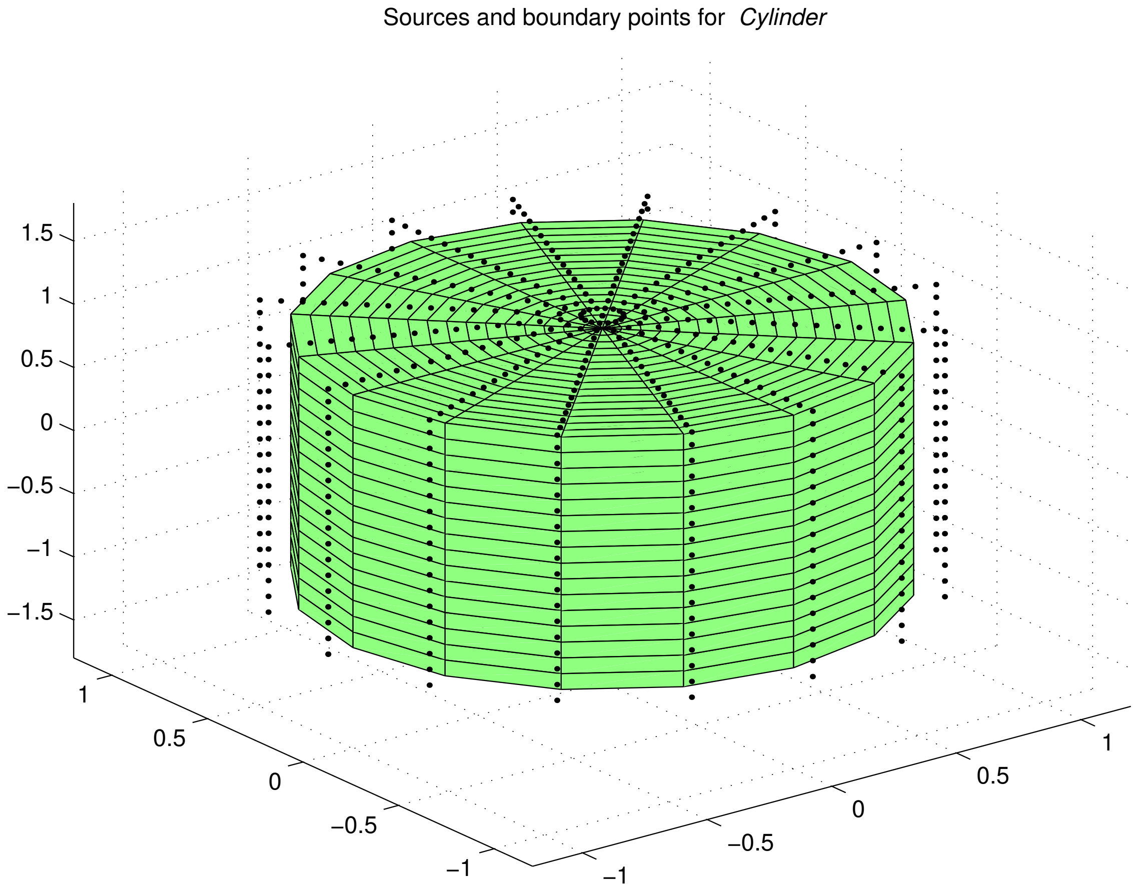

Figure 7: MFS discretization of cylinder.

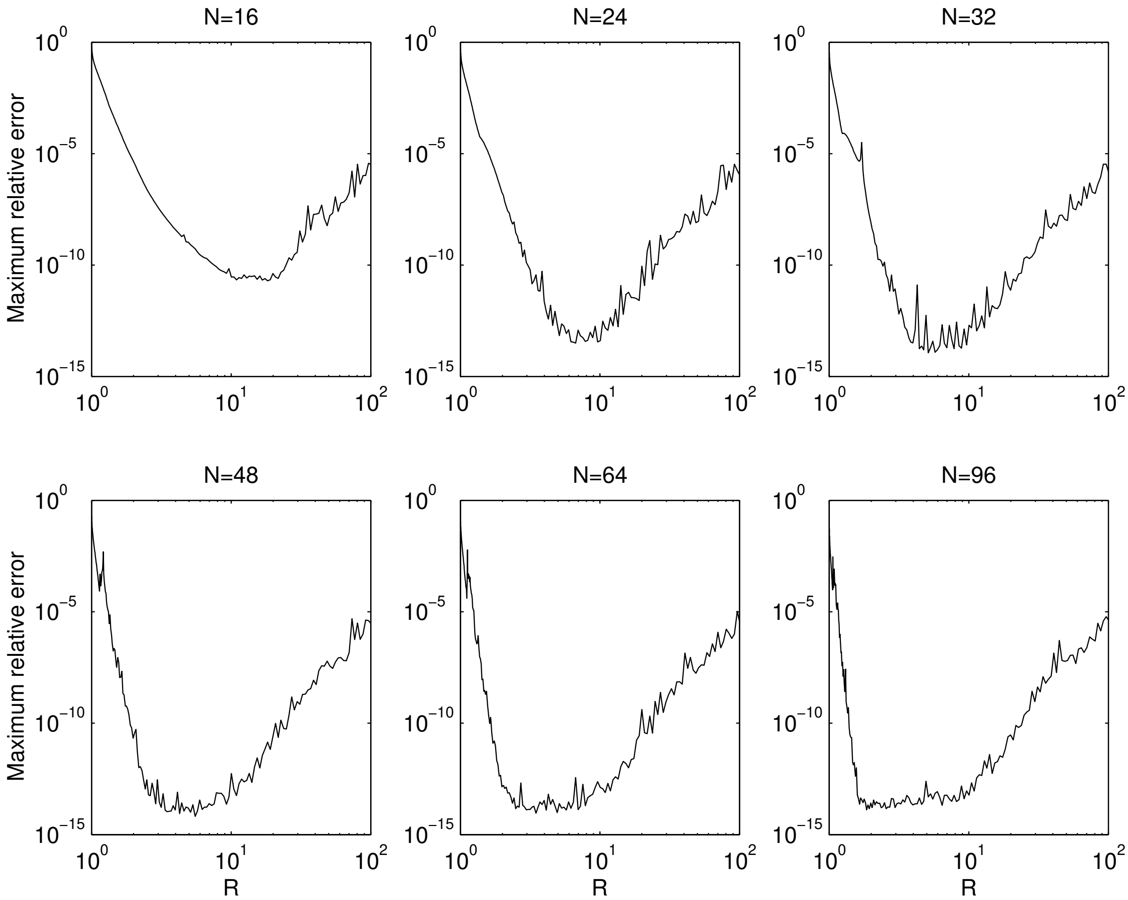

Figure 8: Results for varying distance R and various values of N in the case of the cylinder for Example 1.

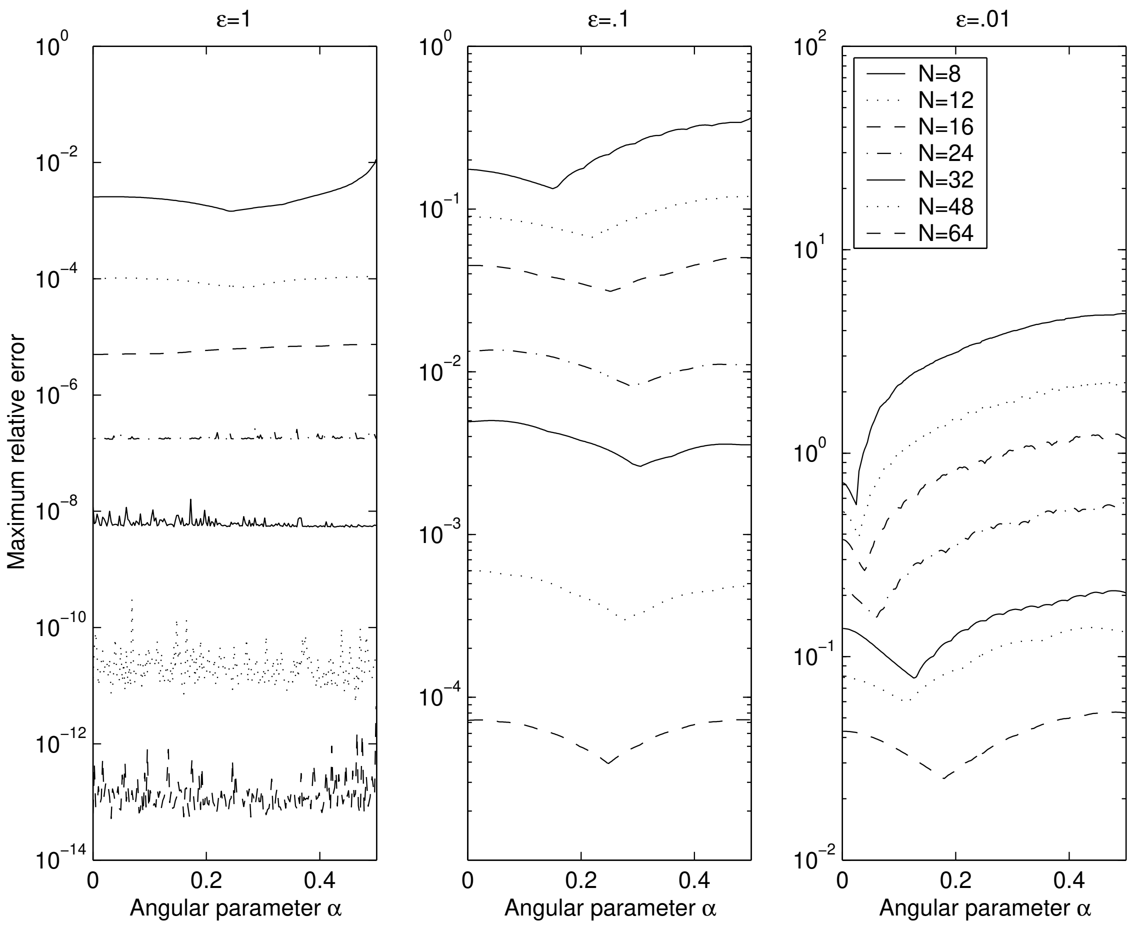

Figure 9: Results for varying parameter α and various values of ϵ in the case of the cylinder for Example 1.

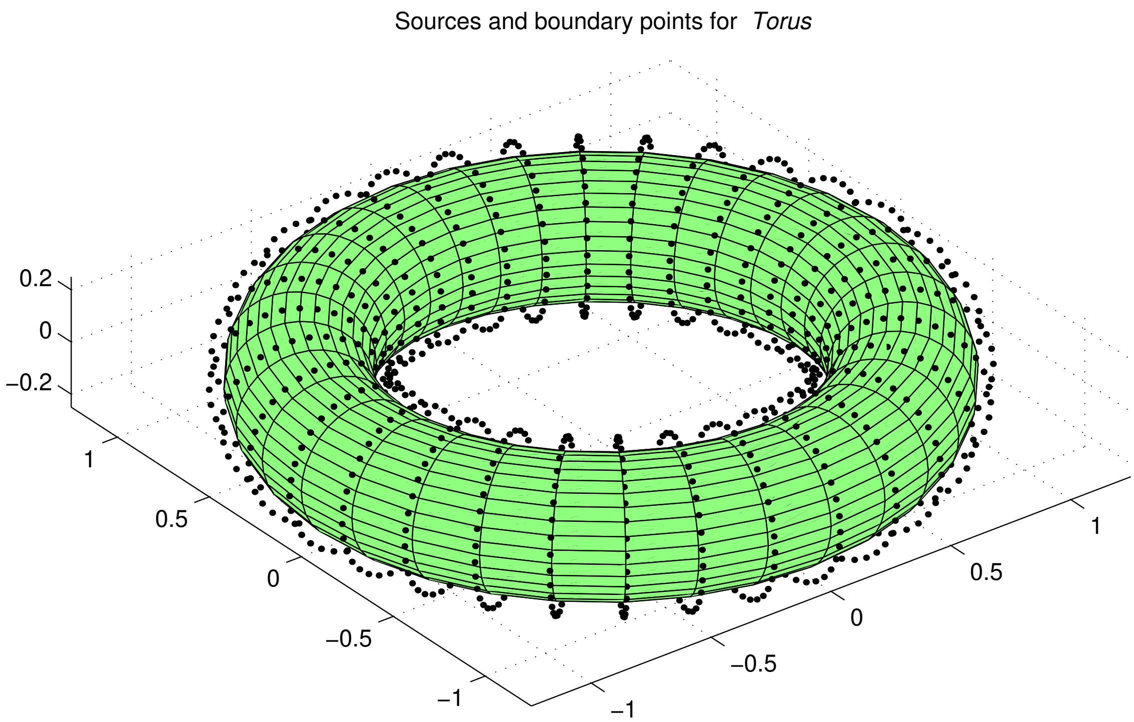

Figure 10: MFS discretization of torus.

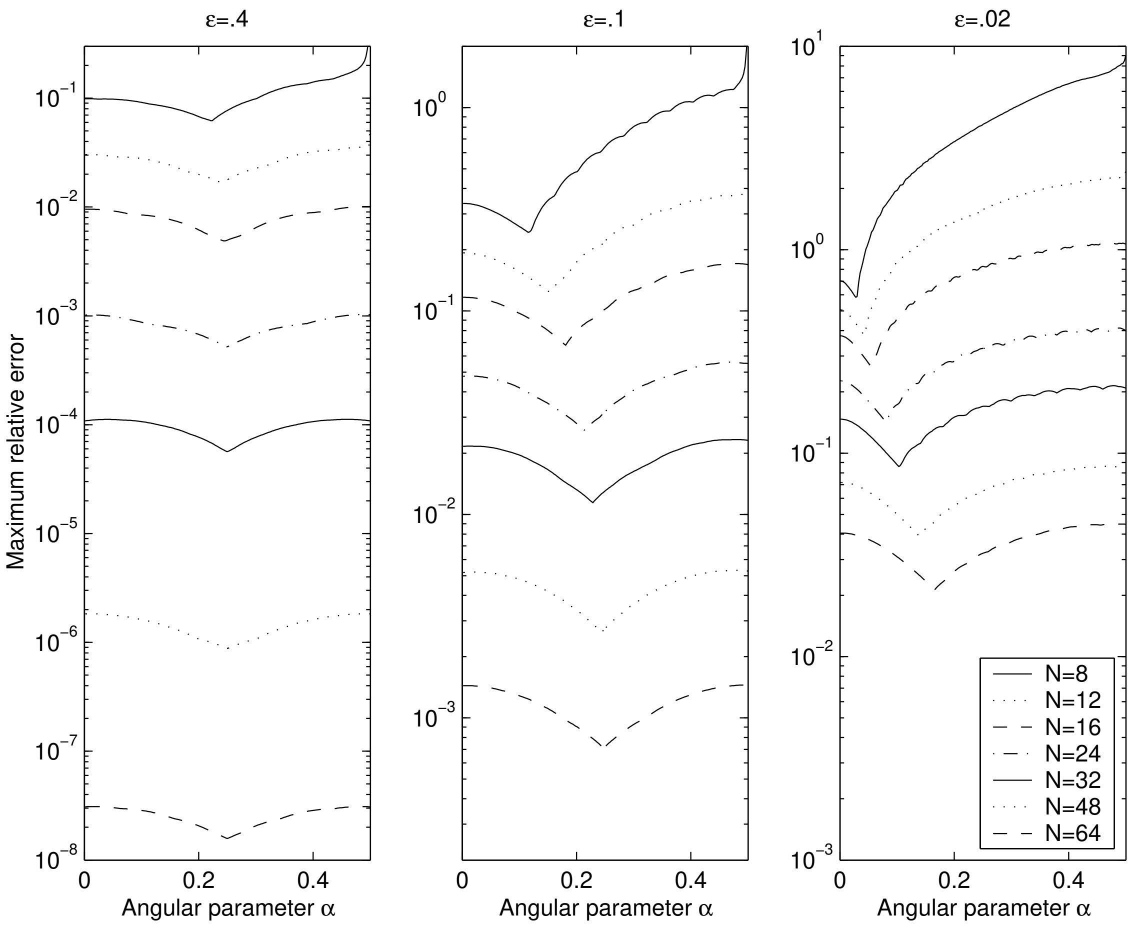

Figure 11: Results for varying parameter α and various values of ϵ in the case of the torus for Example 1.

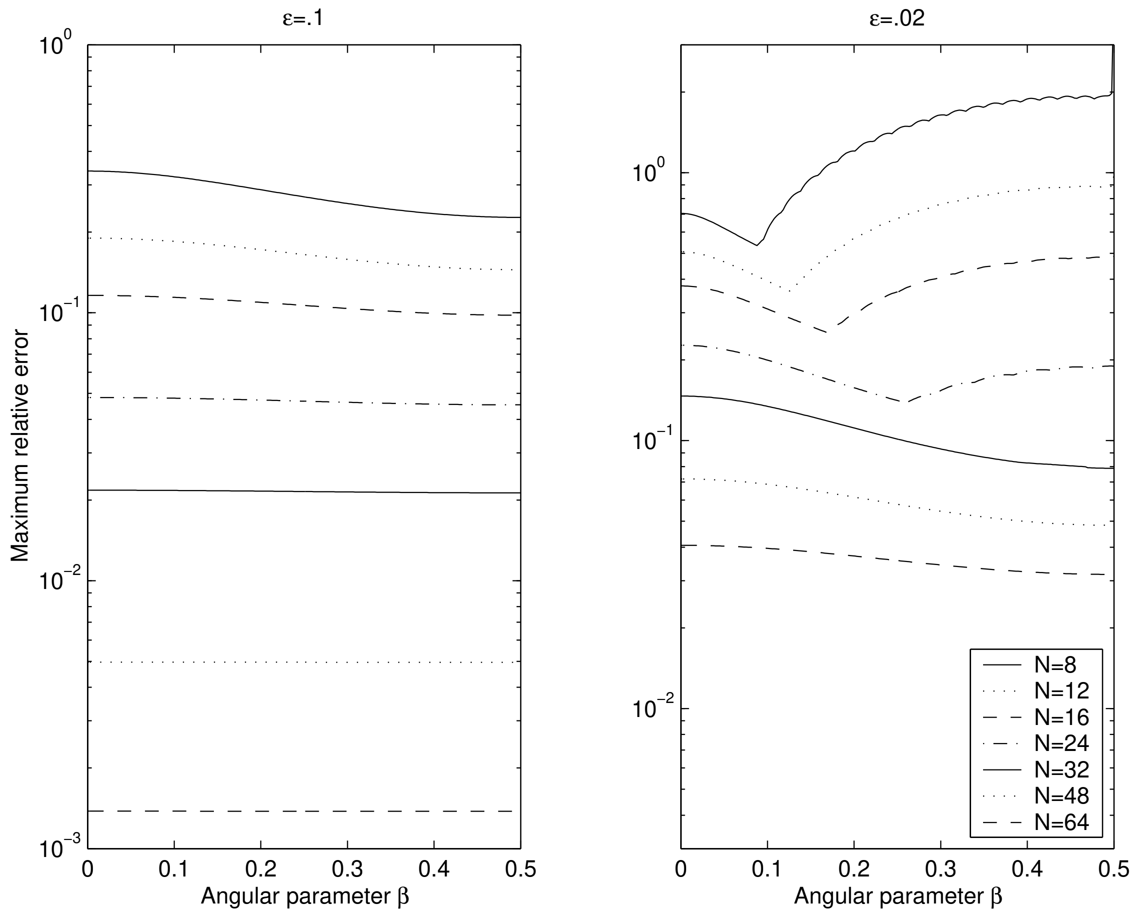

Figure 12: Results for varying parameter β and various values of ϵ in the case of the torus for Example 1.